Voltage-Dependent Corona Discharge-Induced EMI: Insights into Horizontal and Vertical Polarization

Bystrík Dolník

Technical University of Košice, Department of Electric Power Engineering, Mäsiarska 74, 04200 Košice, Slovak Republic; bystrik.dolnik@tuke.sk

Abstract: Corona discharge is a well-known phenomenon in high-voltage systems, presenting both challenges and opportunities in areas such as power transmission, electromagnetic compatibility, and radio interference. This research focuses on analyzing the impact of corona discharge and surface discharges on electromagnetic interference within the frequency range of 30 MHz to 1 GHz. Through experimental measurements, the relationship between spectral maxima, applied voltage, and wave polarization was investigated. The findings indicate that as the applied AC voltage increases, the intensity of electromagnetic interference also rises, with distinct peaks identified in the EMI spectrum. Variations in EMI levels were observed between horizontally and vertically polarized waves. Furthermore, comparisons with regulatory standards revealed instances where interference levels exceeded permissible thresholds.

Keywords: corona discharge; surface discharge; inception voltage; EMC; EMI limits

1 Introduction

Corona discharge is an electrical phenomenon that occurs around object under high-potential gradient (in highly inhomogeneous electric field) when the electric field intensity exceeds the ionization potential of the surrounding air but is not strong enough to cause a complete breakdown. This results in the ionization of the air near the conductor, creating a visible glow, audible noise, radio interference (RI) and, ozone production. The occurrence of corona discharge is influenced by the conductor's geometry, surface conditions, and the surrounding atmospheric conditions. Sharp edges or small-radius conductors are more prone to corona discharge. Corona discharge causes energy losses in high-voltage power transmission systems, reducing efficiency. Corona can generate electromagnetic noise, which interferes with nearby communication systems, leading to issues in electromagnetic compatibility (EMC). The corona discharge produces a hissing or crackling sound, can lead to the production of ozone (O_3) and nitrogen oxides

(NO_x), which may contribute to environmental concerns if sustained over long periods. High humidity, rain, or pollutants in the air can enhance corona effects. Corona discharge is both a challenge and an area of research in power engineering, as it affects energy efficiency, EMC, and equipment longevity [1]. Among the many undesirable effects of corona discharge, particularly in information technology (IT) is electromagnetic interference (EMI). EMI should be understood as degradation in the performance of equipment or transmission channel or a system caused by an electromagnetic disturbance. The EMI generated from high-voltage (HV) overhead power lines can span a wide range of frequencies. This interference originates from various sources, including corona discharges in the air surrounding the conductors, issues with insulator assemblies and hardware, discharges and sparking in stressed areas on insulators, and sparking caused by faulty hardware connections [2].

The formation and characteristics of corona discharge, especially on transmission line conductors, have been extensively studied. Variable atmospheric conditions, such as pressure, temperature, and humidity, significantly affect the corona inception voltage gradient, which in turn impacts corona losses and EMI. Researchers have developed models that incorporate gas discharge theory and numerical calculations to analyze the corona inception voltage gradient, considering factors like conductor arrangement, size, atmospheric conditions, and electrical field distribution [3]. These studies highlight the importance of accurately determining the conditions for corona inception to optimize transmission line performance and minimize corona-related losses [4], [5]. In [6], the authors performed three-year measurements on six-bundled conductors under dry and rainy conditions and suggested changing the elevation correction factor used in engineering design in the USA to 4.5 and 1.5 dB/km separately under dry and raining conditions, which better evaluates coronal loss. Gupta et al. [7] used two years of synchronized phasor measurement data measured on high voltage overhead transmission lines to investigate the influence of weather conditions on corona losses. They found that the most influential weather parameters are air temperature, air pressure, and relative humidity. In [8], the authors used a machine learning model using a recursive elimination method to distinguish positive and negative corona discharges with an accuracy of 0.994.

The impact of corona discharge on EMC should not be underestimated, particularly in relation to RI generated by high-voltage transmission systems. As the adoption of hybrid HV direct current (HVDC) and HV alternating current (HVAC) transmission technologies continues to grow, a comprehensive understanding of corona discharge behavior under the influence of combined alternating current (AC) and direct current (DC) voltages has become critical. Experimental platforms have been established to accurately measure the onset voltage for corona discharge and current pulses across varying conditions, thereby elucidating the intricate interactions among AC and DC voltages, conductor geometry, and the characteristics associated with corona onset [9].

Further studies have explored predictive methodologies for assessing RI levels in HVDC transmission lines using corona cage tests, underscoring the critical importance of considering space charge effects in the development of RI prediction models. The adverse ramifications of corona discharge on the propagation of radio and television signals have received considerable academic attention, particularly concerning interference originating from HV power lines [10]. Additionally, unfavorable weather conditions, such as rain and humidity, worsen the effects of corona discharge, which in turn intensifies EMI and disrupts the reception of radio and television (TV) signals. Consequently, it is essential to implement strategies aimed at mitigating the negative effects of corona discharge to ensure the efficient transmission of radio and TV signals. Standards addressing EMI caused by corona discharge specify a reference measurement frequency of 0.5 MHz. However, alternative frequencies, such as 1 MHz, are also permissible. The choice of 0.5 MHz (or 1 MHz) stems from their representation of higher noise levels in the spectrum and their position between low- and medium-frequency transmission bands [11], [12]. However, modern broadcasting and communication technologies operate at much higher frequencies, making it essential to investigate EMI levels at these higher frequencies, extending up to the GHz range.

In this study, the EMI produced by corona discharge within the frequency range of 30 MHz to 1 GHz are investigated. The motivation for this experimental study stems from the persistent challenges in understanding and mitigating EMI caused by corona discharges in high-voltage systems. Although the phenomenon of corona discharge and its relation to EMI has been recognized in previous studies, several gaps remain in the quantitative characterization of this interference under controlled laboratory conditions, especially concerning conductor geometry, wave polarization, and varying voltage levels. The primary goal of this research was to generate high-fidelity experimental data to support better predictive models and practical mitigation strategies for EMI in power transmission systems. Conducting the experiments in a EMC chamber allowed for isolating corona-related emissions from ambient noise, ensuring accurate and reproducible measurements – an essential requirement for validating future theoretical or computational models. The experiments were conducted using alternating high voltage up to 55 kV applied to rounded copper wires with different diameters and a length of 120 cm. A broadband semi-log antenna was used within an EMC chamber to ensure controlled conditions and accurate data collection.

2 Materials and Methods

The EMC chamber is used to measure EMI from electrical and electronic devices within a frequency range of 30 Hz to 18 GHz. According to the manufacturer, the EMC chamber is completely anechoic up to 2 GHz. The first step of each measurement involved the preparation of the EMC chamber, which included

moving materials supplemented by auxiliary equipment, installing necessary instruments in the EMC chamber, and positioning them appropriately. The placement was carried out in such a way as to ensure the highest possible repeatability of measurements. The instruments were placed on pre-marked spots established during initial measurements.

After appropriately positioning the devices in the EMC chamber, the tested copper conductor, previously shortened to the required length, was connected to the high-voltage part of the transformer using a spherical screw. The spherical design of the screw ensured sufficient homogeneity of the electric field, thereby preventing any discharge activity other than that occurring along the copper conductor. The opposite end of the copper conductor was affixed to the spherical homogenization electrode, which was insulated from the ground. The height of this electrode was adjusted using spacers to ensure it remained horizontal in alignment with the high-voltage spherical screw while the conductor maintained a consistent horizontal position throughout the measurement period. The height of the conductor above the chamber floor was 130 cm. Respecting the dimensions of the EMC chamber, the conductor distance from the radiation measurement mark on the antenna was 235 cm. Figure 1 shows a block diagram of the EMC measurement chain.

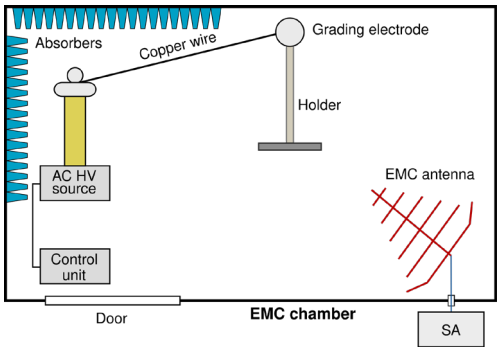

Figure 1

Block diagram of the EMC measurement chain: SA – spectrum analyzer

According to the wiring diagram, the output AC voltage from the regulating AC source (control unit) was connected to the high-voltage part of the transformer. A copper conductor was attached to the HV part of the transformer. The conductor radiation was captured using a broadband biconical logarithmic antenna connected to the spectrum analyzer (SA) using a low-loss cables. The low-loss cables were from Pasternack, type PE302, which are double-shielded and have a maximum operating frequency of 18 GHz. The spectrum analyzer was set to the frequency range from 30 MHz to 1 GHz, while the working frequency is from 20 Hz to 26.5 GHz. The working frequency of the EMC antenna is from 30 MHz to 6 GHz. The attenuation characteristics of the cable and the antenna factor of the used EMC-calibrated antenna were recorded into the SA. The spectrum analyzer

performed the SWEEP (peak) function with twenty repetitions. We used a Peak (MaxPeak) detector to record the maximum value that occurred during the measurement period. This detector detects the highest levels (worst case) because it registers every peak in the measured band during twenty sweeps.

After completing twenty sweeps, the measured data were archived in CSV format. Subsequently, the voltage applied to the conductor was increased by a predefined voltage step of 5 kV. This measurement procedure was repeated up to the maximum voltage of the HV source of 50 kV. We corrected the measured data by a correction factor of −2.121 dB due to the conversion of the measured values to the calibrated antenna distance of 3 m. Results are presented graphically as a frequency dependence of the electric field intensity E expressed in dBμV/m. We investigated EMI measurements generated by corona discharge separately for horizontal and vertical polarization. The original data measured by the spectrum analyzer in CSV format were transformed into text files (*.dat, or *.data) using a shell script under Ubuntu 20.04.6 LTS on a PC with an Intel® Core™ i7-8559U processor and 32 GB RAM. Statistical data analysis was performed in GNU Octave 7.1 using a script created by the author. Before measuring the EMI generated by the copper conductor under AC high voltage, electromagnetic (EM) background (BG) noise measurements were conducted in the EMC chamber. We performed the background noise investigation in the EMC chamber using three scenarios to exclude possible interference from the AC high-voltage transformer and the control unit (CU). The first scenario focused on examining the BG noise in the EMC chamber with the doors open. In this case, electromagnetic waves penetrated through the door into the chamber. During this test, the CU was in a switched-off state.

The second scenario assessed the electromagnetic BG noise after completely closing the chamber doors, ensuring no external interference entered the chamber. Again, the CU remained turned off during this test. The final third scenario examined the BG noise of the EMC chamber after the chamber door was closed and the CU simultaneously switched on to the operating state. At the same time, the CU had a voltage setting of zero volts to capture potential emissions from the unit in the no-load state. The measured values show that the BG noise of the anechoic chamber was unaffected by turning on the control unit. The frequency spectrum with the CU switched on overlaps with the frequency spectrum with the source switched off in the entire frequency range. The same scenario was with the EMC chamber door closed with a maximum AC voltage of 50 kV without a connected conductor on the HV side. Opening the chamber door caused external interference to penetrate the EMC chamber. In the frequency response of the background noise in the anechoic chamber with the door open, six frequency regions appeared where there was a significant increase in the electric field intensity compared to the BG noise with the door closed. The signal detected at a frequency of 95.15 MHz represents the radio broadcast of the commercial station Rádio Expres, transmitted from the Košice-Bankov transmitter located in the

Košice-Sever district of the city. Other frequency regions of increased electric field intensity are due to WiFi and telecommunication signals, as shown in Figure 2. Environmental conditions in the EMC chamber during measurements were as follows: the ambient temperature from 22 °C to 23 °C and relative air humidity from 28 % to 32 %.

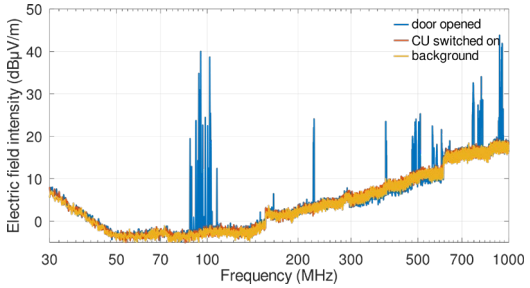

Figure 2
The frequency response of the background EMI: the output voltage of the HV AC source is zero

3 Results and Discussion

Following the EMI background noise assessment in the EMC chamber, measurements of the EMI conductor's radiation were performed for various diameters and applied voltages. First, the EMI generated by the conductor with a diameter of 180 µm was measured, followed by measurements with the other two conductors (850 µm and 2650 µm).

3.1 Frequency Response of Corona Discharges from Wires

The measured frequency spectra of individual conductors were divided into measurements at horizontal polarization of the antenna and subsequently at vertical polarization. Depending on the applied voltages, the frequency spectra are evaluated separately for horizontal (HP) and vertical polarization (VP). Figure 3 shows the frequency spectra of the electric field intensity (EMI radiation) measured at the HP of the antenna for a copper wire with a diameter of 180 µm. Figure 4 shows the frequency spectra for VP of the same wire. The voltage on the copper wire was increased from a minimum value of 5 kV to a maximum value of 55 kV. Because some characteristics overlap, the graphs display only the selected curves for voltages of 5 kV, 10 kV, 20 kV, 30 kV, 40 kV, and 50 kV. It also applies to wires with 850 µm and 2650 µm diameter. Although the measurements were carried out up to a frequency of 1 GHz, in the graphic outputs, the upper limit frequency is up to 400 MHz because the intensity of the electric field did not change from the frequency higher than 400 MHz and copies the course during the measurement of the background response in the EMC chamber.

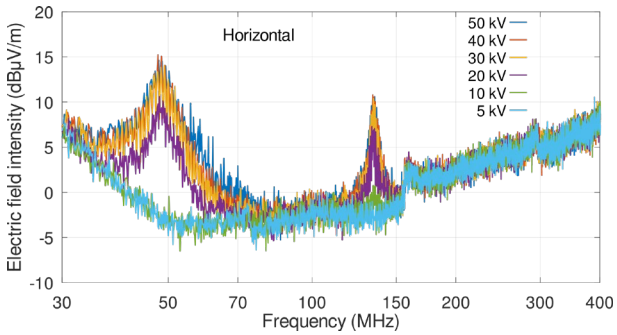

Figure 3

EMI radiation from the 180 μm diameter conductor and horizontally polarized EM waves

In the graph in Fig. 3, two local maxima are evident at 48.43 MHz and 134.76 MHz. The EMI frequency response at a minimum voltage of 5 kV did not show an increase in intensity at any of the frequencies mentioned. The first slight increase in the electric field intensity occurred at an applied voltage of 10 kV and a frequency of 134.76 MHz. At voltages higher than 10 kV, EMI emissions at 48.43 MHz occurred. The local maxima increase with the increasing value of applied voltage. The most significant increase in EMI is at 48.43 MHz.

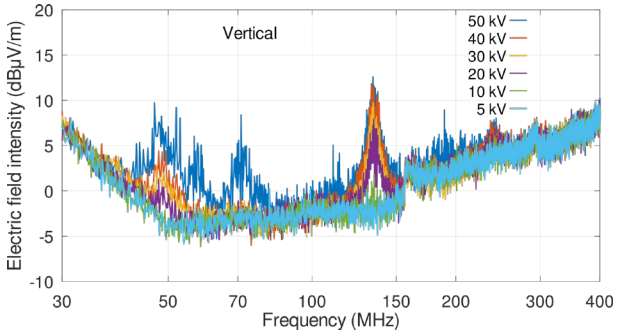

Figure 4

EMI radiation from the 180 μm diameter conductor and horizontally polarized EM waves

After changing the antenna polarization to vertical, there were changes in the EMI amplitudes in the frequency response. No changes appeared at a voltage of 5 kV compared to the EMC chamber's background. At a voltage of 10 kV, a local maximum begins to form with a frequency of 134.76 MHz, as depicted in Fig. 4. A second local maximum at 48.43 MHz and 240 MHz was detected after increasing the voltage to 20 kV. In addition to the two local maxima mentioned, with VP of electromagnetic (EM) waves at a voltage of 50 kV, other significant increases in the electric field intensity occur between 41 MHz and 74 MHz, which did not arise at all at lower voltages.

The graph in Fig. 5 for HP of EM waves and a conductor with a diameter of 850 µm shows three local EMI maxima: 55.87 MHz, 143.49 MHz, and 387.93 MHz. At a voltage of 5 kV, the EMI frequency response copies the background in the EMC chamber. The formation of local maxima begins from a voltage of 10 kV. The EMI frequency response when changing the antenna polarization to vertical (Fig. 6) shows changes compared to the HP of EM waves.

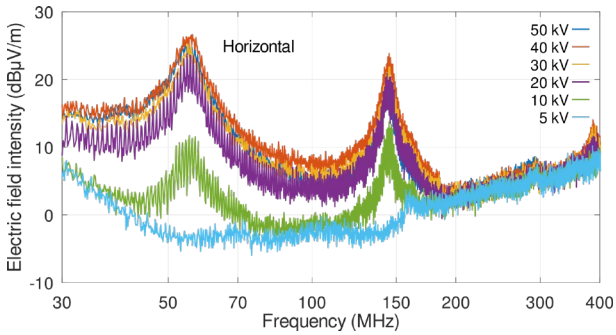

Figure 5

EMI radiation from the 850 µm diameter conductor and horizontally polarized EM waves

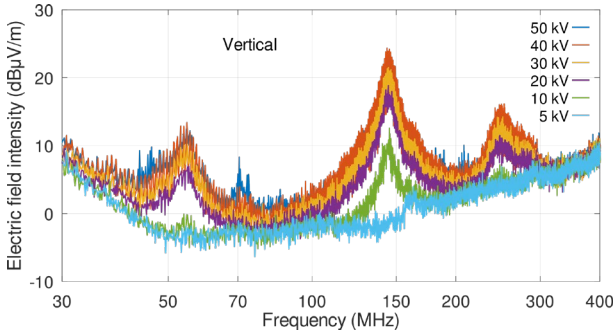

Figure 6

EMI radiation from the 850 µm diameter conductor and vertically polarized EM waves

In VP of EM waves, there is a significant increase in radiation at a frequency of 250.35 MHz, which did not occur when measuring horizontally polarized EM waves. There is also a notable increase in EMI at 143.49 MHz. The EMI emission at this frequency was the second highest in the case of HP, but when measured with the antenna in VP, this frequency is dominant, and the emission is the strongest. In contrast, the EMI at 55.87 MHz, where the emission was the strongest for HP, dropped sharply. Similar to the measurement with the 180 µm diameter conductor and vertical EMI polarization, there is an increase in EMI at 70.41 MHz at the maximum applied voltage, which did not occur at lower voltages.

The frequency response in Fig. 7 shows horizontally polarized EMI radiated by a conductor with a diameter of 2650 µm. The measured waveform shows a local maximum at 57.65 MHz and 143.49 MHz, after which the waveform copies the background of the EMC chamber. The EMI frequency spectra of the largest-diameter conductor for horizontally polarized EM waves replicate the background frequency spectrum of the EMC chamber over the entire range of up to 30 kV. From an applied voltage of 40 kV, a sharp increase in EMI is observed, and subsequently, this radiation increases slightly with increasing applied voltage.

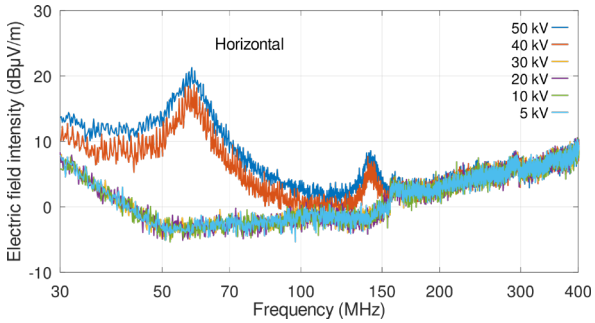

Figure 7
EMI radiation from the 2650 µm diameter conductor and horizontally polarized EM waves

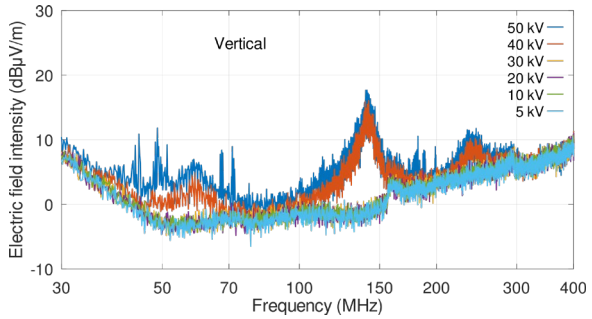

Figure 8
EMI radiation from the 2650 µm diameter conductor and vertically polarized EM waves connections

The change in the frequency response of vertically polarized EMI in Fig. 8 is evident in the maximum measured values of the electric field intensity and the change in the frequency of local maxima. Similar to the case of HP, local maxima began to appear only from voltages higher than 40 kV. For VP, the absolute maximum occurs at 141.1 MHz. The second local EMI maximum is at 239.39 MHz. Similarly, as in the case of the conductor with a diameter of 180 µm and 850 µm, a local maximum at 58.62 MHz arose for the vertical polarization. When comparing the EMI of a 2650 µm diameter conductor with smaller diameter conductors, the local maxima only started to form at a significantly higher voltage than for smaller diameter conductors. This phenomenon is due to the higher corona inception voltage for geometries with a larger radius of curvature.

3.2 Statistical Analysis of EMI Local Maxima

We performed repeated EMI measurements for selected local frequency maxima depending on the applied voltage. Due to a more accurate determination of local maxima and statistical evaluation, we changed the measurement mode on the SA to the EMI receiver. We obtained 2001 electric field intensity values for each voltage level in the time series. The sampling rate during the EMI measurement is 10 ms. With a more accurate measurement in EMI receiver mode, the position of the local maxima on the frequency axis differs from the previous local maxima shown in Fig. 3 to 8. Figure 9 shows the statistics of the electric field intensity for horizontally and vertically polarized EMI simultaneously for the local maximum of 64.51 MHz and 64.6 MHz using the violinplot (VP) function. The VP is an attractive and effective way of showing multiple distributions simultaneously. A VP shows peaks in the data, visualizes the distributions of numerical data, and displays summary statistics and the density of each variable. In the colored areas, in Figs. 9 to 12 and Figs. 17 and 18, the black circle represents the median, and the line through the median shows the interquartile range (from the first quartile to the third quartile). Wider sections of the VP represent a higher probability that the random variable will take on a given value; thinner sections represent a lower probability. In addition, the shape of the distribution allows one to distinguish between a single distribution and a superposition of multiple distributions.

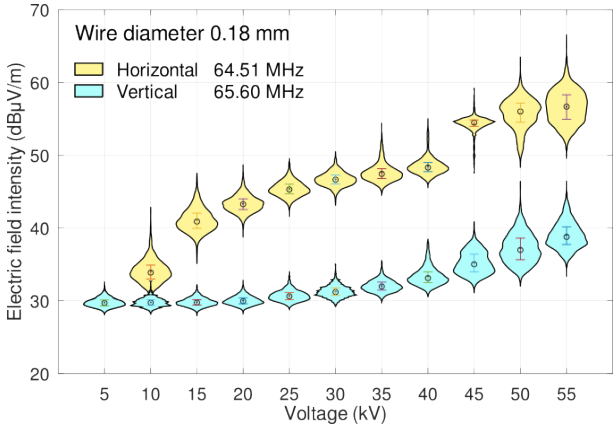

Figure 9

Electric field intensity for HP and VP EMI with a frequency of 64.51 MHz and 65.6 MHz

From the graph in Fig. 9, one can see that horizontally polarized EMI is greater than vertically polarized EMI from an applied voltage higher than 5 kV. From the graph in Fig. 9, one can see that, for example, for VP, the electric field intensity values are within one distribution up to 40 kV of applied voltage, while at higher applied voltages, it is a superposition of two to three distributions. Similarly, the interquartile range at applied voltages above 40 kV has widened. Figure 10 shows statistics for horizontally and vertically polarized EMI at 163.5 MHz. In this case,

the dependence of EMI on the applied voltage is similar for horizontally and vertically polarized EMI components. The increase in EMI has an exponential trend. Within the voltage range from 5 kV to 35 kV, the EMI values are almost identical. From a voltage of 40 kV, the horizontally polarized EMI is slightly higher than the vertically polarized EMI, with the difference in EMI values being in the range of tenths of a dB to 1 dB.

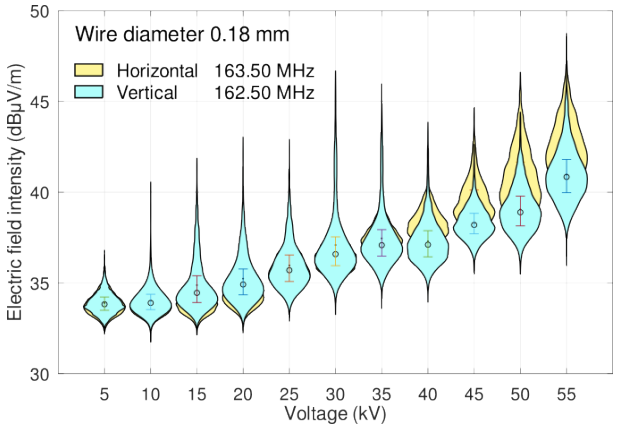

Figure 10
Electric field intensity for HP and VP EMI with a frequency of 163.5 MHz and 162.5 MHz

The graph in Fig. 11 represents the electric field intensity for horizontally and vertically polarized EMI with a frequency of 55.87 MHz and a conductor with a diameter of 850 µm. In this case, the frequency response of corona discharges is similar to that in Fig. 9. At applied voltages of 5 kV and 10 kV, the frequency response follows the background of the EMC chamber. From an applied voltage of 15 kV, corona discharges are detected, which is 5 kV more than in the case of a conductor with a diameter of 180 µm. The formation of corona discharges at higher applied voltage is due to a larger radius of curvature of the conductor, see, Fig. 19. Figure 12 shows electric field intensity for horizontally and vertically polarized EMI with frequencies of 57.65 MHz and 56.97 MHz and a conductor with a diameter of 2650 µm. In the HP of EMI, the formation of corona discharges from the applied voltage of 35 kV is clearly visible. It is confirmed that the inception voltage of corona discharges increases with the increase in the radius of curvature of the wire. All measured electric field intensity values generated from wires with three different diameters (180 µm, 850 µm, and 2650 µm) at various applied voltages from 5 kV to 55 kV are freely available in [13].

Figure 9 demonstrates that for horizontally polarized EM waves, the EMI limit for Class B is exceeded at applied voltages of 15 kV and higher, while for Class A, the limit is surpassed at applied voltages of 45 kV and above. Conversely, for vertically polarized EMI, neither Class A nor Class B exceeds the limits across the entire range of applied voltages.

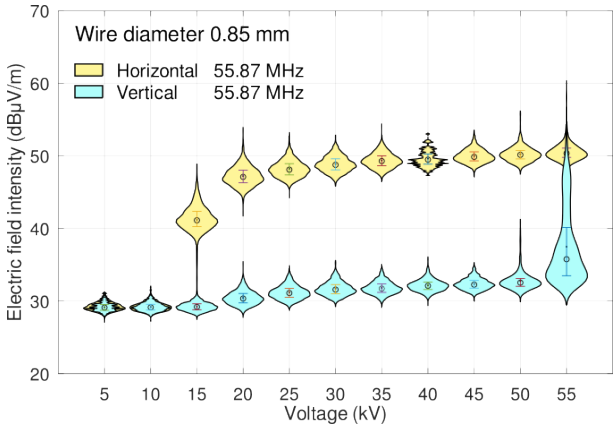

Figure 11

Electric field intensity for HP and VP EMI with a frequency of 55.87 MHz

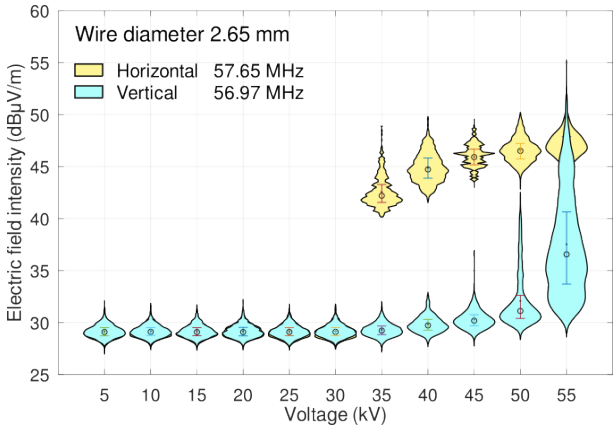

Figure 12

Electric field intensity for HP and VP EMI with a frequency of 57.65 MHz and 56.97 MHz

The comparison of measured EMI against the specified limits is based on average EMI values. However, when considering the whole data set of measured EMI values for each applied voltage, the limits are exceeded at lower applied voltages. This behavior is attributed to the significant variability in the statistical distribution of EMI, which is visually represented through violin plots in Figures 9 to 12. The difference ΔE between the maximum measured electric field intensity and the average electric field intensity across all voltage levels, as calculated using equation (1), ranges from 2.2 dB to 9.3 dB.

$$\Delta E = E_{max} - E_{mean} \tag{1}$$

In (1), E_{max} represents the maximum measured EMI, and E_{mean} denotes the mean EMI value. Table 1 shows the differences between the maximum and average

EMI values for different wire diameters and selected local frequency maxima. In Table 1, ΔE_{min} is the minimum difference, and the ΔE_{max} denotes the maximum difference within the applied voltage range.

Table 1
Calculated EMI differences between maximum and mean electric field intensities

Frequency (MHz)	Wire diameter (mm)	Polarization	ΔE_{min} (dBμV/m)	ΔE_{max} (dBμV/m)
64.51	0.18	H	2.7	9.3
65.60	0.18	V	2.2	8.6
163.50	0.18	H	2.5	6.6
162.50	0.18	V	2.8	9.1
55.87	0.85	H	1.9	9.2
55.87	0.85	V	2.1	17.5
57.65	2.65	H	1.9	7.5
56.97	2.65	V	2.0	14.2

The statistical graphs in Fig. 9 to 12 show that horizontally polarized EMI dominates. This fact can be explained by the geometric orientation of the interference source. The interference source is a corona wire oriented horizontally, looking at the base. This corona wire can be considered as a transmitting antenna, and due to its orientation, the EMC antenna will effectively capture the EM waves generated by the wire when horizontally polarized.

3.3 Frequency Response of Surface Discharges

The investigation of discharges on the glass surface had the same instrumentation and a different electrode configuration. The high-voltage part of the transformer was connected to the upper electrode located on a glass plate with dimensions 15 cm × 17 cm and a thickness of 5 mm, under which a second grounded electrode was fixed. Both electrodes are cylindrical in shape. The upper electrode has a diameter of 54 mm, a height of 58 mm, and a radius of curvature in the lower part of 4 mm. The lower electrode has a diameter of 50 mm, a height of 15 mm, and a radius of curvature of 7.5 mm. A large-diameter wire was used to connect the high-voltage part of the transformer to prevent corona discharges on this connecting wire, which could distort the measurement results. The discharge activity on this wire was checked using a UV camera. Due to the significant discharge activity on the glass surface occurring at lower voltages than in the previous case (EMI radiation on wires), the maximum applied voltage for surface discharges was 20 kV, and the minimum voltage was 2 kV. The voltage was increased from the minimum to the maximum value in steps of 2 kV.

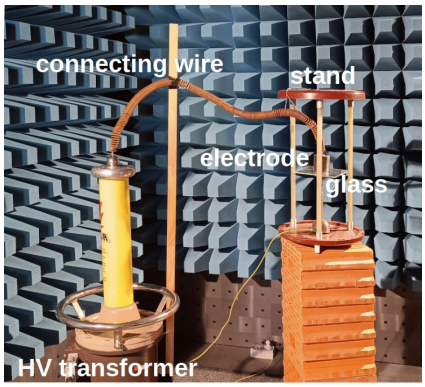

Figure 13
Connection of the electrode configuration to HV transformer

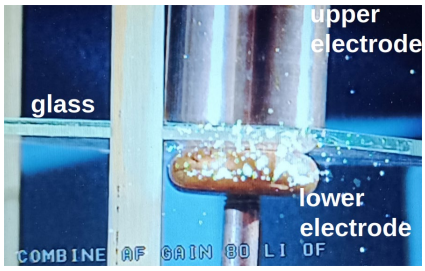

Figure 14
Detection of surface discharges using the DayCor camera

EMI generated by discharges on the glass surface in horizontal polarization has different frequency spectra than the interference generated by the corona around the wires. The EMI frequency response in Fig. 15 shows that the interference increased monotonically with increasing voltage from the applied voltage of 2 kV. The most significant increase in EMI is when the voltage from 16 kV is increased to the maximum voltage of 20 kV. A greater number of local peaks appear in the frequency spectrum of surface discharges than in the frequency spectra of wires. The peaks detected when measuring discharges on the surface are located at frequencies: (38.57, 72.36, 82.38, 143.98, and 268.62) MHz. As the frequency increases, the local maxima decrease.

After changing the antenna polarization to vertical, the frequency spectra changed. In Fig. 16, one can see that the fundamental difference is in the change in response to an increase in the applied voltage from 16 kV to 20 kV when there was no significant increase in interference as in the case of horizontal polarization.

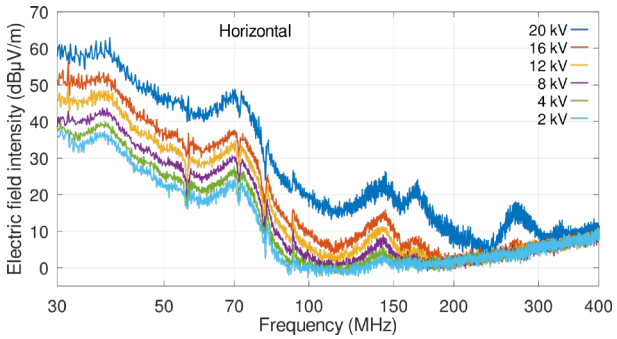

Figure 15

EMI radiation from surface discharges and horizontally polarized EM waves

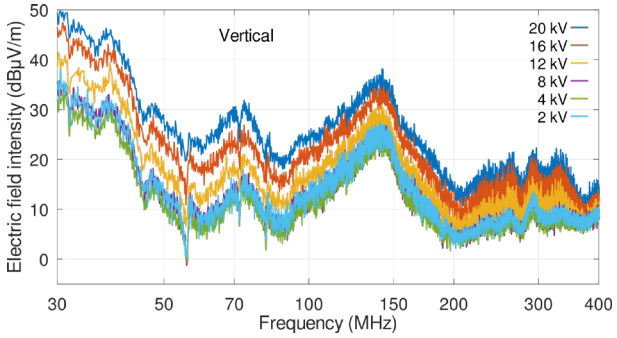

Figure 16

EMI radiation from surface discharges and vertically polarized EM waves

Moreover, there is no peak at the frequency of 268.62 MHz. The interference is most intense at a frequency of 30.49 MHz and a voltage of 20 kV. This local maximum is followed by a sharp decrease in the electric field intensity, during which local maxima form at frequencies of 55.38 MHz and 80.93 MHz. Then, a significant local maximum forms at a frequency of 142.52 MHz.

3.4 Statistical Analysis of Surface Discharges EMI Local Maxima

For the statistical analysis of EMI generated by surface discharges, graphs for two selected local maxima are presented. Fig. 17 shows the statistics of the local maximum at 38.57 MHz and Fig. 18 at 143.98 MHz. Surface discharges are detected from a minimum applied voltage of 2 kV. In both cases, the EMI is higher for vertically polarized EMI, and the electric field intensity increases monotonically with increasing applied voltage. According to CISPR standards, the limits for both classes A and B are exceeded already at an applied voltage of 8 kV to 10 kV.

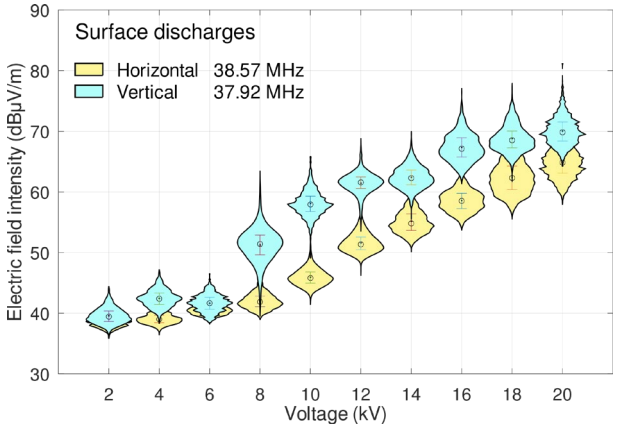

Figure 17
Electric field intensity for HP and VP EMI with a frequency of 38.57 MHz and 37.92 MHz

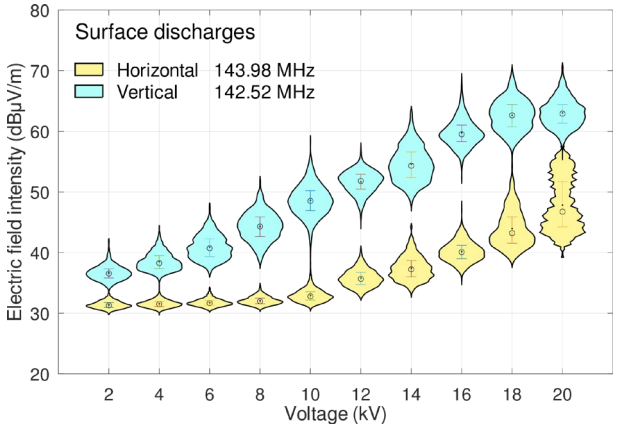

Figure 18
Electric field intensity for HP and VP EMI with a frequency of 143.98 MHz and 142.52 MHz

Therefore, it is necessary to use suitable measures to reduce EMI either on the side of the interfering source or the victim side using suitable effective shielding materials [14]. When information must be transmitted through electromagnetic fields through the air, e.g., between power plants of different types for network stability [15], transmission frequencies greater than 300 MHz should be used. EMI emissions measured on wires indicate that interference above 300 MHz is insignificant.

Fig. 19 shows the dependence of the corona inception voltage (CIV) on the radius of the conductor. Experiments in the EMC chamber were carried out over a long period (four months). During this period, the air pressure varied. The lowest air pressure in the laboratory was 99.9 kPa, the highest 102 kPa. The graph in Fig. 19 shows the calculated values of the CIV according to the empirical Peek's law,

where the parameter is air pressure. The AC corona inception field strength (kV_p/cm) is expressed as:

$$E_{c,p} = 31.5 \cdot m \cdot \delta \left(1 + \left(\frac{0.3054}{\sqrt{\delta \cdot r}}\right)\right) \tag{2}$$

and the corresponding CIV

$$V_{c,p} = r \cdot E_{c,p} \cdot ln\left(\frac{h}{r}\right) \tag{3}$$

In equations (2) and (3), m is the roughness factor of the conductor surface ($m \leq 1$), δ is the relative air density, r is the conductor radius (in cm), and h is the height of the conductor above the ground (cm). The relative air density is

$$\delta = \frac{p}{p_0} \cdot \frac{273+t_0}{273+t} \tag{4}$$

where p_0 is the standard atmospheric pressure (kPa), p is the actual pressure (kPa), $t_0 = 20$ °C, and t is the ambient temperature (°C) [16], [17], [18].

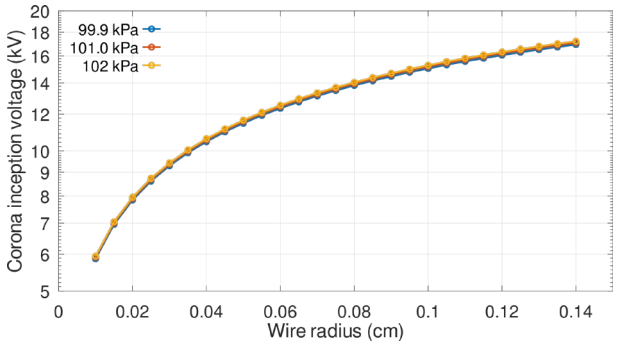

Figure 19

Dependence of the ICV on the radius of a smooth conductor, the parameter is air pressure

According to the statistical graphs in Fig. 9 to 12 for wires with different diameters, the ICV of a wire with a diameter of 0.18 mm is between 5 kV and 10 kV (Fig. 9), for a diameter of 0.85 mm between 10 kV and 15 kV and 2.65 mm between 30 kV and 35 kV. By comparing with the calculated CIV values in Table 2, the EMI values are similar to the measured values for wires with a diameter of 0.18 mm and 0.85 mm (peak values). The calculated CIV value for a wire with a diameter of 2.65 mm is lower than the measured one. The calculated CIV values in Table 2 are given in the format kV_p / kV, where kV_p denotes peak value, kV r.m.s. value and the slash has no division meaning.

All measured electric field intensities generated by surface discharges at various applied voltages from 2 kV to 20 kV are freely available in [13].

Table 2
Calculated corona inception voltage of a smooth conductor (m = 0.95); the parameter is air pressure; the slash has no division meaning

Wire diameter (mm)	Air pressure (kPa)		
	99.9	101	102
	Corona inception voltage (kV_p / kV)		
0.18	5.61 / 3.97	5.65 / 4.0	5.69 / 4.02
0.85	10.74 / 7.6	10.82 / 7.65	10.90 / 7.7
2.65	16.63 / 11.76	16.77 / 11.86	16.90 / 11.95

As mentioned above, at applied voltages above 40 kV, the interquartile range of the measured electric field intensity is wider compared to lower applied voltages. Since the measurement setup and procedure remained unchanged throughout the measurement period, and the conductor with a different diameter was replaced only, one can argue that all measured data are consistent. It confirms the relatively narrow interquartile range and the position of the median within this range, as well as the margin of error (MoE). The MoE was calculated as $z \cdot \sigma \cdot n^{-0.5}$, where z = 1.96 is the level of confidence (95%), σ denotes the standard deviation, and n represents the size of the sample. In summary, the calculated margin of error value for all three used conductors is 0.02, and the maximum value is 0.22. For surface discharges, the corresponding margin of error is 0.05 and 0.19.

Conclusions

This study has explored the effects of corona discharge on EMI across a wide frequency range of 30 MHz to 1 GHz. Key findings from the research include the observation that EMI radiation from corona and surface discharges increases with higher applied AC voltages. Local peaks in the EMI spectrum were identified, showing a dependence on the applied voltage. Differences in EMI levels were also noted between horizontally and vertically polarized emissions. Additionally, experiments revealed that surface discharges emit stronger radiation compared to corona discharges from wires, even though surface discharge testing was conducted at lower applied voltages. In addition to contributing empirical data, the experiment was necessary to explore practical implications – such as the frequency thresholds above which corona-induced EMI becomes negligible (e.g., above 300 MHz) – that can guide engineers in optimizing communication systems operating in proximity to high-voltage infrastructure.

This study provides new insights, particularly by identifying dominant frequency bands of interference and highlighting the more pronounced effects of horizontally polarized emissions. These findings offer direct relevance for the design of high-voltage components and compliance with EMC standards. When comparing the measured EMI values to the limits specified by standards CISPR 11/EN 55011 and CISPR 22/EN 55022 for Class A and Class B devices, results indicate that these limits exceed at higher voltage levels, particularly for horizontally polarized

emissions. The study also lays the groundwork for further investigations into environmental factors (e.g., humidity, temperature, and pressure), and material-based mitigation methods. By establishing a reliable experimental baseline, this work enables targeted follow-up research and model development, reinforcing its originality and long-term applicability.

Acknowledgement

This work was supported by the Scientific Grant Agency of the Ministry of Education, Research, Development and Youth of the Slovak Republic and the Slovak Academy of Sciences [grant number 1/0380/24]; the Slovak Research and Development Agency [grant number APVV-22-0115]; and the Cultural and Educational Grant Agency of the Ministry of Education, Research, Development and Youth of the Slovak Republic [grant number 008TUKE-4/2019].

References

[1] A. Alidemaj, I. Bula: The negative effects of the corona effect on the propagation of radio and TV waves, IFAC-PapersOnLine, Vol. 55, No. 39, 2022, pp. 342-345, doi: 10.1016/j.ifacol.2022.12.049

[2] TR CISPR 18-1, Technical report, Radio interference characteristics of overhead power lines and high-voltage equipment – Part 1: Description of phenomena, 2010, IEC, Ed. 2.0

[3] D. Fahmi, H. A. Illias, H. Mokhlis, I. M. Yulistya Negara: Negative DC corona patterns for different wire particle geometries in air insulation, Alexandria Engineering Journal, Vol. 73, 2023, pp. 635-649, doi: 10.1016/j.aej.2023.04.068

[4] A. Maglaras, T. Kousiouris, F. Topalis, L. A. Maglaras, K. Giannakopoulou: Optimization of Corona onset and breakdown voltage of small air gaps stressed by DC and impulse voltages, Eurocon 2013, Zagreb, Croatia, 2013, pp. 1207-1214, doi: 10.1109/EUROCON.2013.6625134

[5] C. Tejada-Martinez, F. P. Espino-Cortes, S. Ilhan, A. Ozdemir: Optimization of Radio Interference Levels for 500 and 600 kV Bipolar HVDC Transmission Lines, Energies, Vol. 12, No. 16, Art. No. 3187, 2019. doi: 10.3390/en12163187

[6] S. Huang, L. Ha, Y. Liu, The altitude correction term of the corona loss on alternating-current transmission lines, Energy Reports, Vol. 9, pp. 2149-2152, 2023, doi: 10.1016/j.egyr.2022.12.071

[7] P. K. Gupta, K. Tuttelberg, and J. Kilter, Weather dependency of corona losses on 330 kV overhead transmission lines, International Journal of Electrical Power & Energy Systems, Vol. 155, p. 109537, 2024, doi: 10.1016/j.ijepes.2023.109537

[8] H. I. Uckol and S. Ilhan, Characterization of DC corona discharge current pulses using high-frequency measurement techniques, Measurement, Vol. 218, p. 113154, 2023, doi: 10.1016/j.measurement.2023.113154

[9] Z. Ma, J. Xia, X. He, Y. Zhou, Z. He, Q. Li, X. Bian: Experimental and numerical study on corona onset threshold under combined AC-DC voltages in Wire-Plane electrodes, International Journal of Electrical Power & Energy Systems, Vol. 143, p. 108479, 2022, doi: 10.1016/j.ijepes.2022.108479

[10] A. Carsimamovic, A. Mujezinovic, S. Carsimamovic, Z. Bajramovic, M. Kosarac, K. Stankovic: Analyzing of AC Corona Discharge Parameters of Atmospheric Air, Procedia Computer Science, Vol. 83, p. 766-773, 2016, doi: 10.1016/j.procs.2016.04.165

[11] TR CISPR 18-2, Technical report, Radio interference characteristics of overhead power lines and high-voltage equipment – Part 2: Methods of measurement and procedure for determining limits, 2017, IEC, Ed. 3.0

[12] CISPR 11:2015, Industrial, scientific and medical equipment – Radio-frequency disturbance characteristics – Limits and methods of measurement, 2015, CISPR, Ed. 6.1

[13] B. Dolník (2025), Characterization of Electric Discharge-Induced EMI, Mendeley Data, V1, doi: 10.17632/fv4dv38skn.1

[14] J. Zbojovský, M. Pavlík, I. Kolcunová, J. Kurimský, R. Cimbala: Investigation of Shielding Materials, for the Purpose of Shielding Electromagnetic Fields. Acta Polytechnica Hungarica, Vol. 20, No. 11, 2023, pp. 49-62, doi: 10.12700/APH.20.11.2023.11.4

[15] I. Diahovchenko, I. Yevtushenko, M. Kolcun, Z. Čonka, T. Zahorodnia1, P. Vasyleha: Demand-Supply Balancing in Energy Systems with High Photovoltaic Penetration, using Flexibility of Nuclear Power Plants. Acta Polytechnica Hungarica Vol. 20, No. 11, 2023, doi: 10.12700/APH.20.11.2023.11.8

[16] L. Chen, J. M. K. MacAlpine, X. Bian, L. Wang, Z. Guan: Comparison of methods for determining corona inception voltages of transmission line conductors. Journal of Electrostatics, Vol. 71, No. 3, 2013, pp. 269-275, doi: 10.1016/j.elstat.2012.11.020

[17] K. Tonmitr, T. Ratanabuntha: Comparison of Power Loss Due to Corona Phenomena Model with Peek's Formula in High Voltage 115 kV and 230 kV System. Procedia Computer Science, Vol. 86, 2016, pp. 385-388, doi: 10.1016/j.procs.2016.05.037

[18] 15. J.-R. Riba, W. Larzelere, J. Rickmann: Voltage Correction Factors for Air-Insulated Transmission Lines Operating in High-Altitude Regions to Limit Corona Activity: A Review. Energies, Vol. 11, No. 7, 2018, p. 1908, doi: 10.3390/en11071908